Nanoscale Rotary Motors Driven by Electron Tunneling

Boyang Wang, Lela Vuković, and Petr Král*

Department of Chemistry, University of Illinois at Chicago, Chicago, Illinois 60607, USA

(Received 23 February 2008; published 31 October 2008)

We examine by semiclassical molecular dynamics simulations the possibility of driving nanoscale rotary motors by electron tunneling. The model systems studied have a carbon nanotube shaft with covalently attached "isolating" molecular stalks ending with "conducting" blades. Periodic charging and discharging of the blades at two metallic electrodes maintains an electric dipole on the blades that is rotated by an external electric field. Our simulations demonstrate that these molecular motors can be efficient under load and in the presence of noise and defects.

DOI: 10.1103/PhysRevLett.101.186808 PACS numbers: 85.65.+h, 45.40.−f, 84.50.+d, 85.35.Gv

Biological molecular motors transport various cellular components and provide the motility to biosystems [1]. For example, kinesin can burn adenosine triphosphate (ATP) and generate *linear* motion along cytoskeleton [2]. Other proteins, driven by proton gradients across membranes, mechanically *rotate* flagella to propel bacteria [3]. Biological motors can also be used *in vitro* [4], where they have many potential applications in powering of motile nanosystems and manipulating colloidal nanostructures [5].

Molecular motors can be powered by optical [6–8], electrical [9,10], and chemical means [11] and other ratchetlike principles [12]. At the macroscale, electronic driving is the most efficient method of powering motors [13]. At the nanoscale, electric current driving could in principle be realized by resonant or nonresonant *electron tunneling* [14,15]. It was shown that tunneling can induce periodic vibrational [16] and translational motions in molecules [17]. But it is intriguing to transform nanoscale vibrations into a concerted rotary motion, so the use of tunneling for driving might be rather limited.

In this Letter, we explore if electron tunneling could drive *rotary* nanoscale machines. We design rather simple nanoscale rotary motors powered by electron tunneling, and use molecular dynamics (MD) simulations to study their possible activity. For the best control of these nanodevices, it might be convenient to separately control tunneling (blade charging) and driving (rotation powering) processes. Therefore, we test separately motors with *neutral* and *charged* electrodes, where these processes have a different amount of dependency.

The first type of motor is displayed in Fig. 1. Its shaft is formed by a (12,0) carbon nanotube (CNT) [18], which could be fixed into CNT bearings [19]. Three (six) stalks, formed by polymerized iceane molecules with saturated bonds [20] are attached to the shaft at an angle of 120° (60°) with respect to each other. The asymmetry of the iceane stalks causes the 6-fullerene rotor to have C_3 symmetry, which, from the points of fullerenes, is close to the C_6 symmetry. The stalks are chosen to have the length of $l \approx 2$ nm, in order to prevent nonresonant electron tunneling from the blades to the shaft [14]. The energies of their electronic states should also prevent the electron transfer along the stalks by resonant tunneling [15]. The blades are formed by molecules with conjugated bonds (fullerenes), covalently attached at the top of the stalks. In principle, such a hybrid molecular rotor could be synthesized by cycloaddition reactions [21].

A homogeneous electrostatic field $\mathcal{E}$, oriented along the vertical z direction, is used for periodical charging and discharging of the blades by electron tunneling from two neutral metallic electrodes. The rectangular electrodes have the width of $w \approx 4$ Å and the length of $l \approx 75$ Å. This length and the overall neutrality of the electrodes should decrease the effect of transient charging and discharging on the motor driving. The field $\mathcal{E}$ powers the system by rotating the formed *dipole* p of the rotor that is on average orthogonal to the field direction.

We set the distance d between the electrodes and the blades (barrier width) from the length of the tunneling time τ. The tunneling processes must be completed when the

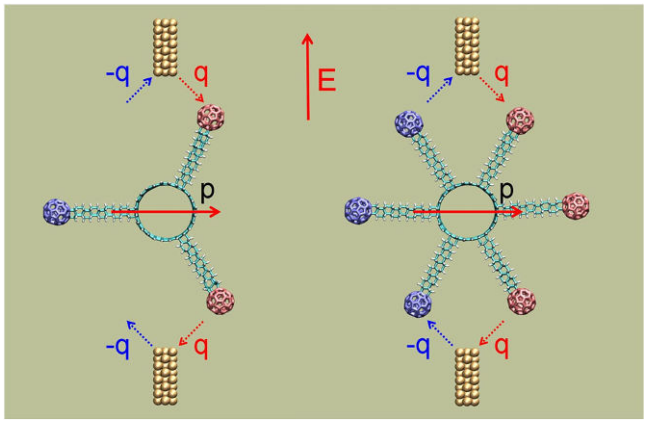


FIG. 1 (color online). Tunneling-driven nanoscale motors with three (left) and six (right) fullerene blades. In an external homogeneous electric field $\mathcal{E}$ oriented along the vertical z direction, the electron tunneling from the neutral electrodes to the blades maintains an electric dipole p on the rotor, which is on average orthogonal to the field direction. This dipole is unidirectionally rotated by the electric field (movie in Ref. [29]).

 © 2008 The American Physical Society

blade, moving with the rotation speed of the motor, is below the electrode. If these conditions are met, the motor dynamics should not be sensitive to τ. In order to roughly estimate τ, we model the tunneling process in a potential double well, where both the electrode and the blade are assumed to be two 1 nm-wide quantum wells separated by a 4 eV-high square potential barrier (typical ionization potential) with a variable width d. We simply take for τ the inverse energy splitting between the lowest energy (symmetric and asymmetric) states of this double well. The obtained time τ depends exponentially on the distance d; we obtain $\tau = 0.95$ and 8.1 ps for $d = 7.5$ and 10 Å, respectively. Since tunneling during recharging of the blade from $\mp e$ to $\pm e$ actually involves two electrons, τ should be twice as large, in the first approximation. We assume that the electrons get from the electrode to the blade or back within this time, and the blade has one charge that stays there due to the homogeneous field $\mathcal{E}$.

We fix the minimum distance between the bottom of the electrode and the top of the blade (fullerene) to $d_{\min} = 7.5$ Å. When the blade passes below the electrode, the stalk rotates over an angle of $\theta = 180w/\pi l \approx 12°$. Assuming that the two-electron tunneling at the distance of $d_{\min}$ takes $\tau \approx 1.9$ ps, the angular velocity of the motor should not be larger than ≈ 60 ps per round, in order to complete the tunneling process when the blade is below the electrode. In the MD simulations, we model the tunneling process by assuming that the electron transfers instantaneously when the fullerene gets closer than $d_{\min}$ to the electrode. Since the blade vibrates, this happens shortly before it gets below the center of the electrode. At this point we briefly stop the simulation and homogeneously recharge the fullerene by *two* electrons, from $\mp e$ to $\pm e$ at the anode and cathode, respectively. Since each blade only carries a single charge, electron-electron coupling is less important. The charge of the electrodes is assumed to be instantaneously replenished as well.

We assume that proper reservoirs can hold the electrodes neutral in the presence of the field $\mathcal{E}$, and neglect their possible polarization. The electrochemical potential on the anode is $\mu_{\text{ano}} = E_F + e\mathcal{E}z_{\text{ano}}$, where E_F is the Fermi energy. In the tunneling process, the anode should neutralize first the positive blade (fullerene) ion by providing one electron to the blade's highest occupied molecular orbital (HOMO) state. Then the anode should change the blade to a negatively charged ion with a half filled lowest unoccupied molecular orbital (LUMO) state. The electron energies in these states are $E_{\text{LUMO/HOMO}} + e\mathcal{E}z_{\text{blade}}$, where $E_{\text{LUMO/HOMO}}$ are the respective LUMO/HOMO energies. The electrochemical potential μ_{ano} should be such that only these two processes occur at the anode and the opposite processes occur at the cathode. One could also envision asymmetric systems, with charge of one sign passing in one half of the rotation.

We simulate the motor activity with the NAMD package [22] based on the CHARMM27 force field [23]. We estimate parameters of atoms in aliphatic groups and the nanotube from similar atom types, and add them to the CHARMM27 force field. In order to thermalize the motors during the simulations while preventing the unphysical loss of their angular momenta [5], we couple them with a small Langevin damping, $\gamma_{\text{Lang}} = 0.01$ ps^{-1}, to the reservoir at the temperature of $T = 300$ K.

During the simulations, we leave the CNT rotor free to vibrate, but place three fixed dummy atoms along its axis to fix its radial motion. Two larger fixed dummy atoms are also placed outside each of the two CNT ends in order to fix its longitudinal motion. Since the motor is symmetric, it can be rotated in any direction. To set it in motion, we can simply rotate it by one round in the chosen direction. This charges the blades accordingly, and the motor will continue to rotate in that direction by Coulombic forces acting on the charged blades.

We study the efficiency of the motors under external load. The average driving torque exerted on the rotor is $\mathcal{T}_{\text{drive}} = \mathcal{E}r_e \sum_{i=1}^{n} e_i \langle \sin(\theta_i) \rangle$, where e_i are the charges on the blades, r_e is their distance from the rotor axis, and $\langle \sin(\theta_i) \rangle$ are the average directional sines between the stalks and the field direction. A *steady-state* rotation of the motor can be established if the driving torque $\mathcal{T}_{\text{drive}}$ is balanced by the damping torque $\mathcal{T}_{\text{damp}}$. The latter has an internal component $\mathcal{T}^{\text{in}}_{\text{damp}}$, which represents damping of the system alone, and the external component $\mathcal{T}^{\text{ex}}_{\text{damp}}$, which represents the external load of the system. In steady-state situations, the average angular momentum L of the rotor is time independent,

$$\dot{L} = \dot{L}_{\text{drive}} + \dot{L}_{\text{damp}} = \mathcal{T}_{\text{drive}} - \mathcal{T}^{\text{in}}_{\text{damp}} - \mathcal{T}^{\text{ex}}_{\text{damp}} = 0. \quad (1)$$

We can approximately describe the internal damping by $\mathcal{T}^{\text{in}}_{\text{damp}} = L\tau_{\text{in}}^{-1} = I\omega\tau_{\text{in}}^{-1}$, where τ_{in} is the internal angular-momentum relaxation time, I is the momentum of inertia, and ω is the angular frequency of the rotor. The relaxation time, $\tau_{\text{in}}^{-1} \approx \tau_{\text{Lang}}^{-1} + \tau_{\text{phon}}^{-1}$, can be formally decomposed into Langevin and phonon components. The latter describes how selected vibration (phonon) modes, associated with coherent motions of the stalks, damp the angular momentum of the rotor [7]. In fact, these vibration modes mediate the rotor-field coupling [9]. In this process, these vibration modes can retain a significant amount of the transferred angular momentum, which they damp by scattering from the fixed electrodes.

In order to test the efficiency of the motors, we need to stabilize their steady-state rotation at different ω. In MD simulations, this can be achieved by having the external damping $\mathcal{T}^{\text{ex}}_{\text{damp}}$ dependent on ω. We use the linear dependence $F^{\text{ex}}_{\text{damp}} = c_d\omega$, realized by applying two tangential forces with opposite orientations, but the same magnitudes proportional to ω, to the opposite sides of the shaft. Then, the motors rotate in a stable way and sustain a certain load, beyond which they stop.

We can easily calculate the efficiency of the motors. The input power is the work done by the driving torque per unit

time, $P_{\text{input}} = \mathcal{T}_{\text{drive}}\omega$. It is also equal to the change of the Coulombic energy per unit time of the charges carried by the blades between the electrodes, $P_{\text{input}} = UI = \mathcal{E}d_eI$, where $d_e = 2r_e \approx 6$ nm is the distance over which the charges are carried by the blades and $I = 6e\omega/2\pi$ is the related electric current (for the 3-blade system). The output power of the motor is the work exerted on the loading torque, $P_{\text{output}} = \mathcal{T}^{\text{ex}}_{\text{damp}}\omega$. Therefore, the motor efficiency is given by

$$\eta = \frac{P_{\text{output}}}{P_{\text{input}}} = \frac{\mathcal{T}^{\text{ex}}_{\text{damp}}\omega}{\mathcal{T}_{\text{drive}}\omega} = \frac{\mathcal{T}^{\text{ex}}_{\text{damp}}}{\mathcal{T}_{\text{drive}}}. \quad (2)$$

If the internal damping can be neglected, $\mathcal{T}^{\text{ex}}_{\text{damp}} \gg \mathcal{T}^{\text{in}}_{\text{damp}}$ (high loading limit), we obtain in the steady state that $\mathcal{T}_{\text{drive}} = \mathcal{T}^{\text{ex}}_{\text{damp}} + \mathcal{T}^{\text{in}}_{\text{damp}} \approx \mathcal{T}^{\text{ex}}_{\text{damp}}$ and $\eta \to 1$.

In Fig. 2, we evaluate η as a function of c_d and $\mathcal{E}$ for the 3-fullerene and 6-fullerene motors. Both systems have about the same driving torques if the field $\mathcal{E}$ in the 3-fullerene system is twice as large than that in the 6-fullerene system. Note that the first rotor is an ion, while the second rotor is a neutral molecule. Therefore, the total Coulombic forces on the first rotor are nonzero, but this does not change its driving. Each point is obtained by calculating ω from 20 steady-state rotations lasting in total 1–4 ns. In the limit of high loading, $c_d > 1.5$ nN ps, the efficiency saturates, but $\eta \leq 0.5$–0.8, due to substantial phonon damping. The limiting value is rather high, $\eta \to 0.85$, for the 3-fullerene system with less phonon modes than the 6-fullerene system. At lower loading, η is controlled by the internal dissipation, which removes all the angular momentum from the rotor in the limit of $c_d \to 0$. Since no work is generated, we obtain $\eta \to 0$, in analogy to macroscopic electric motors [13].

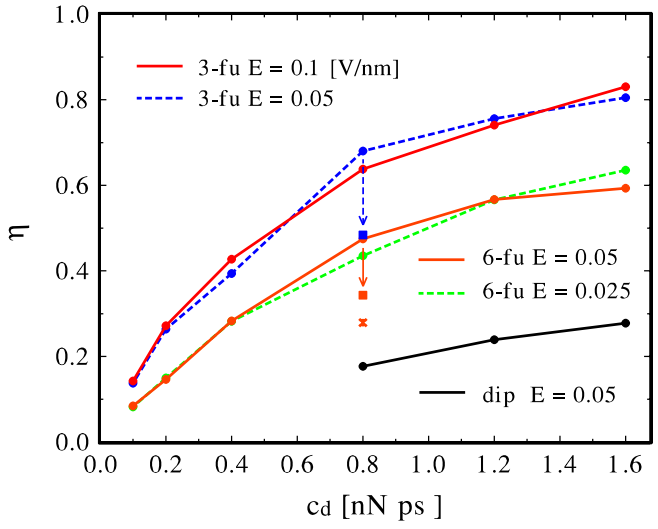


FIG. 2 (color online). The efficiency η for the 3-fullerene and 6-fullerene motors at different damping c_d. At larger c_d the efficiency grows and becomes stabilized, but $\eta_{3\text{-}fu} > \eta_{6\text{-}fu}$. In the presence of mistakes ($c_d = 0.8$ nN ps and $\mathcal{E} = 0.05$ V/nm), the 3-fullerene motor has $\eta = 48.38\%$ (one mistake in charging per rotation), the 6-fullerene has $\eta = 34.32\%$ (two nonconsecutive mistakes in charging per rotation) and $\eta = 27.89\%$ (perfect charging, but one of the six blades is missing). The efficiency of the more complex dual-blade system η_{dip} is even smaller.

The described motors and their dynamics are in many ways an idealization of the real situation. Mistakes in structure or/and relative positioning of the molecular components, inevitably present in these systems, can generate noise during the tunneling (random charges and timing), accompanied by the variation of the driving forces. Shot noise can be generated even in perfect structures, due to thermal fluctuations. To estimate the consequences, we study motors with relatively large errors, where one and two (nonconsecutive) charging events are randomly absent per cycle in the 3-fullerene and 6-fullerene motors, respectively. Alternatively, we remove one of the six stalks in the 6-fullerene motor. The results presented in Fig. 2 show that the efficiency decreases by 10%–20%, but the dynamics is preserved. The potentially dangerous time-dependent fluctuations in the motor performance due to these errors could be eliminated in motors with many *brushlike* blades attached to the stalk and coupled to long electrodes.

The presence of neutral electrodes, which cannot interfere with tunneling and driving processes, is another idealization. We thus examine motors with charged electrodes that generate *local electric fields* superimposed on the homogeneous field $\mathcal{E}$. Let us consider first that the electrodes in the motors from Fig. 1 are oppositely charged. Then right before the tunneling, the strong Coulombic coupling between the oppositely charged blade and the adjacent electrode brings the system to a global minimum of its potential energy. However, immediately after the

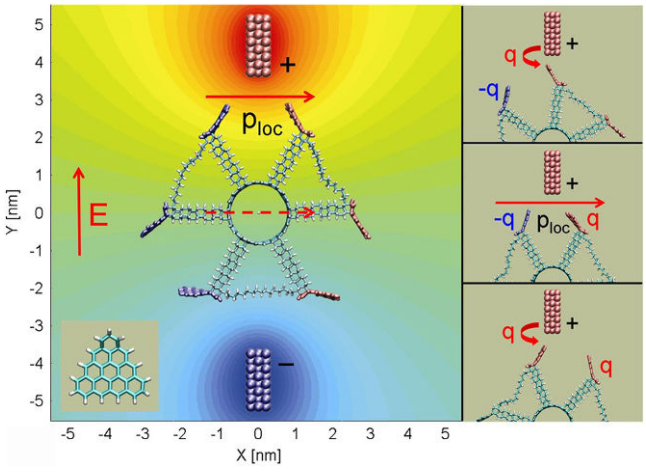


FIG. 3 (color online). Tunneling-driven molecular motor with three dual blades. The inset (left down) shows the blade in detail. (Right) The activity of the blades during the dual-tunneling process. (Top) Before the first tunneling, where both half-blades are attracted; (middle) after the first tunneling, where the electrode interacts with a local dipole p_{loc} formed by the blades; (bottom) after the second tunneling, where both blades are repulsed forward (movie in [29]).

tunneling, the system switches to the state of global energy maximum. Therefore, the tunneling point is a point of *instability*. After the tunneling event, the rotor can move in *any* direction, unless the Coulombic forces on the other blades are significant or the rotor carries a large angular momentum.

This instability can be removed in the system shown in Fig. 3. Each of its three blades is split into two half-blades that are *charged stepwise* by electron tunneling during the motor rotation. The half-blades are formed by planar aromatic molecules with triangular shapes (left inset), covalently attached to the iceane stalks. Each half-blade has a total charge of $\pm e$, where the atomic charges are calculated *ab initio* [24]. Since the two sides of the triangles in neighboring half-blades point to each other, the electric dipole p_{loc} formed when the two half-blades are oppositely charged is rather local. They are blocked from joining each other by n-$C_{16}H_{32}$ alkane chains. Each (metallic) electrode, of the $4 \times 14.3 \times 77.4$ Å size, has 400 atoms homogeneously charged with the total charge of $\pm 2e$. Since the charged electrodes are long, the charged and vibrating blades practically do not experience any side forces that might destabilize the rotation. As before, we set $d_{\text{min}} \approx 7.5$ Å and instantaneously charge each half-blade when it gets closer than d_{min} to the electrode. The homogeneous field is $\mathcal{E} = 0.05$ V/nm.

In the right-hand insets of Fig. 3, we show three configurations of the two half-blades during their stepwise charging by tunneling. In this process, the potential energy surface of the Coulombic blade-electrode coupling is changed, so the energy minima and maxima are spatially shifted one from another. Before the first tunneling event, both half-blades are attracted to the electrode (top inset of Fig. 3). After this event, they form the dipole p_{loc} that translates along the charged electrode and continues in driving the rotor in the same direction (middle inset of Fig. 3). The instability is further suppressed by keeping the dipole p_{loc} local, since its both charges on the two flexible half-blades are at about the same distance to the electrode most of the time. After the tunneling event to the second half-blade is over, both half-blades repel from the electrode in the same direction with comparable strength and continue to rotate the motor (bottom inset of Fig. 3). The forces acting on the other blades reinforce the unidirectional motion of the rotor. Note that Coulomb blockade effects [25], due to repulsion of electrons on the two half-blades, might be important during the half-blade charging by tunneling in realistic systems.

We again calculate the motor efficiency η at different damping constants c_d. The output power P_{output} is found from Eq. (2). However, the input power needs to be modified to the presence of charged electrodes,

$$P_{\text{input}} = UI = (\mathcal{E} d_e + \Delta\phi_{\text{elec}})I. \quad (3)$$

We can easily find the potential difference $\Delta\phi_{\text{elec}} \approx 0.6$ V generated by the charged electrodes over the distance $d_e \approx 6$ nm. The dependence $\eta = f(c_d)$ plotted in Fig. 2 shows that this motor is about 3 times less efficient than the 3-fullerene system. This drop in efficiency is caused by a large dissipation of the angular momentum into the vibration modes of the six flexible charged blades and the three loose alkyl chains. The efficiency could be improved by directly fixing the blades on larger rigid rotors. These results demonstrate the feasibility of driving nanoscale systems [26–28] by tunneling rotary motors.

*pkral@uic.edu

[1] M. Schliwa, *Molecular Motors* (Wiley-VCH Verlag, Weinheim, 2003).
[2] M. J. Schnitzer and S. M. Block, Nature (London) **388**, 386 (1997).
[3] T. Atsumi, L. Mccarter, and T. Imae, Nature (London) **355**, 182 (1992).
[4] R. K. Soong *et al.*, Science **290**, 1555 (2000).
[5] B. Wang and P. Král, Phys. Rev. Lett. **98**, 266102 (2007).
[6] J. Vacek and J. Michl, Proc. Natl. Acad. Sci. U.S.A. **98**, 5481 (2001).
[7] P. Král and H. R. Sadeghpour, Phys. Rev. B **65**, 161401(R) (2002).
[8] S. Tan, H. A. Lopez, C. W. Cai, and Y. Zhang, Nano Lett. **4**, 1415 (2004).
[9] P. Král and T. Seideman, J. Chem. Phys. **123**, 184702 (2005).
[10] J. E. Green *et al.*, Nature (London) **445**, 414 (2007).
[11] T. R. Kelly, H. De Silva, and R. A. Silva, Nature (London) **401**, 150 (1999).
[12] R. D. Astumian, Science **276**, 917 (1997).
[13] H. Auinger, Power Eng. J. **15**, 163 (2001).
[14] K. V. Mikkelsen and M. A. Ratner, Chem. Rev. **87**, 113 (1987).
[15] P. Král, Phys. Rev. B **56**, 7293 (1997).
[16] H. Park, J. Park, A. K. L. Lim, E. H. Anderson, A. P. Alivisatos, and P. L. McEuen, Nature (London) **407**, 57 (2000).
[17] C.-C. Kaun and T. Seideman, Phys. Rev. Lett. **94**, 226801 (2005).
[18] J. Han, A. Globus, R. Jaffe, and G. Deardorff, Nanotechnology **8**, 95 (1997).
[19] J. Cumings and A. Zettl, Science **289**, 602 (2000).
[20] C. A. Cupas and L. Hodakowski, J. Am. Chem. Soc. **96**, 4668 (1974).
[21] D. Tasis, N. Tagmatarchis, A. Bianco, and M. Prato, Chem. Rev. **106**, 1105 (2006).
[22] J. C. Phillips *et al.*, J. Comput. Chem. **26**, 1781 (2005).
[23] M. Karplus *et al.*, J. Phys. Chem. B **102**, 3586 (1998).
[24] M. J. Frisch *et al.*, computer code GAUSSIAN 03, revision D.01, Gaussian, Inc., Wallingford, CT, 2004.
[25] C. Livermore, C. H. Crouch, R. M. Westervelt, K. L. Campman, and A. C. Gossard, Science **274**, 1332 (1996).
[26] R. Dreyfus *et al.*, Nature (London) **437**, 862 (2005).
[27] Y. Shirai *et al.*, J. Am. Chem. Soc. **128**, 4854 (2006).
[28] M. Manghi, X. Schlagberger, and R. R. Netz, Phys. Rev. Lett. **96**, 068101 (2006).
[29] See EPAPS Document No. E-PRLTAO-101-043846 for three supplementary movies. For more information on EPAPS, see http://www.aip.org/pubservs/epaps.html.